International Journal of Nanomedicine

Dovepress
open access to scientific and medical research

Open Access Full Text Article

ORIGINAL RESEARCH

The Application of 2d Mxene Nanosheet -Based Thermosensitive Gel Delivery System Loaded with Cisplatin and Imiquimod for Lung Cancer

Yuwei Ma[1,2,*], Tao Jiang[1,2,*], Rong Zhang[1], Fei Liu[3], Shilong Song[1,2], Huijun Zhang[4], Jingwen Huang[1], Zelai He[1,2]

[1]The First Affiliated Hospital of Bengbu Medical University & Tumor Hospital Affiliated to Bengbu Medical University, Bengbu, 233004, People's Republic of China; [2]Department of Radiation Oncology, the First Affiliated Hospital of Bengbu Medical University & Tumor Hospital Affiliated to Bengbu Medical University, Bengbu, 233004, People's Republic of China; [3]Anhui Province Key Laboratory of Clinical and Preclinical Research in Respiratory Disease, Molecular Diagnosis Center, Department of Pulmonary and Critical Care Medicine, the First Affiliated Hospital of Bengbu Medical University, Bengbu, 233004, People's Republic of China; [4]Department of Cardiothoracic Surgery, Huashan Hospital of Fudan University, Shanghai, 200040, People's Republic of China

*These authors contributed equally to this work

Correspondence: Zelai He; Jingwen Huang, Email hezelai@alumni.sjtu.edu.cn; he.ze.lai@163.com; byyfyhjw@163.com

Introduction: Lung cancer's high incidence and dismal prognosis with traditional treatments like surgery and radiotherapy necessitate innovative approaches. Despite advancements in nanotherapy, the limitations of single-treatment modalities and significant side effects persist. To tackle lung cancer effectively, we devised a temperature-sensitive hydrogel-based local injection system with near-infrared triggered drug release. Utilizing 2D MXene nanosheets as carriers loaded with R837 and cisplatin (DDP), encapsulated within a temperature-sensitive hydrogel-forming PEG-MXene@DDP@R837@SHDS (MDR@SHDS), we administered in situ injections of MDR@SHDS into tumor tissues combined with photothermal therapy (PTT). The immune adjuvant R837 enhances dendritic cell (DC) maturation and tumor cell phagocytosis, while PTT induces tumor cell apoptosis and necrosis by converting light energy into heat energy.

Methods: Material characterization employed transmission electron microscopy, X-ray photoelectron spectroscopy, phase transition temperature, and near-infrared thermography. In vitro experiments assessed Lewis cell proliferation and apoptosis using CCK-8, Edu, and TUNEL assays. In vivo experiments on C57 mouse Lewis transplant tumors evaluated the photothermal effect via near-infrared thermography and assessed DC maturation and CD4+/CD8+ T cell ratios using flow cytometry. The in vivo anti-tumor efficacy of MDR@SHDS was confirmed by tumor growth curve recording and HE and TUNEL staining of tumor sections.

Results: The hydrogel exhibited excellent temperature sensitivity, controlled release properties, and high biocompatibility. In vitro experiments revealed that MDR@SHDS combined with PTT had a greater inhibitory effect on tumor cell proliferation compared to MDR@SHD alone. Combining local immunotherapy, chemotherapy, and PTT yielded superior anti-tumor effects than individual treatments.

Conclusion: MDR@SHDS, with its simplicity, biocompatibility, and enhanced anti-tumor effects in combination with PTT, presents a promising therapeutic approach for lung cancer treatment, offering potential clinical utility.

Keywords: 2D Mxene, drug delivery system, hydrogel, lung cancer

Introduction

Lung cancer is a malignant tumor with the highest morbidity and mortality rate in the world. It is the second most common cancer in men and women after prostate cancer and breast cancer, respectively. The 5-year survival rate for lung cancer is 22%.[1] The two main histological types of lung cancer are small cell lung cancer and non-small cell lung cancer (NSCLC), with the latter accounting for almost 80% of lung cancer patients.[2] Surgery, radiotherapy, and chemotherapy are widely used in the clinical treatment of lung cancer, but these treatments have some limitations.[3–5] Lung cancer

Received: 13 November 2023
Accepted: 17 May 2024
Published: 25 May 2024

tissues are usually located close to vital organs, which makes surgery difficult, and the surgical margins are prone to residual lesions.[6,7] Pulmonary radiotherapy is ineffective for large tumors and can cause severe radiation pneumonia.[8] Intravenous chemotherapy can cause non-specific distribution of drugs in the body and insufficient doses of drugs to act on tumor cells, resulting in poor efficacy and major side effects.[9–11] Therefore, exploring safe and effective local treatment strategies is necessary to reduce systemic toxicity and side effects and improve drug concentration and efficacy at the tumor site.

In recent years, lung cancer-related research has been increasingly dedicated to exploring new treatments, such as immunotherapy and photothermal therapy (PTT).[12] Immunotherapy kills tumor cells by stimulating the host's immune response to the cells. $CD8^+$ T lymphocytes (also called T cells) are considered one of the most effective tumor immune killer cells.[13] Dendritic cells (DCs) are the most important antigen-presenting cells (APCs) used to activate T cells.[14] However, DCs are affected by the tumor immunosuppressive microenvironment; they are basically in an immature and non-functional state and, thus, cannot produce an immune response to kill tumor cells.[15,16] Toll-like receptor (TLR) agonists, which can activate TLRs expressed on DCs to induce their maturation, show great potential in tumor therapy. PTT is a non-invasive treatment. It induces apoptosis and necrosis of tumor cells by converting light energy into heat energy and controls local tumor lesions.[17–19]

Although PTT and immuno-chemotherapy have certain advantages, systemic administration of drugs not only inhibits bone marrow cell production but also causes immune-related adverse reactions due to an overactive immune system.[20,21] Here, local administration emerges as an ideal mode of drug delivery. As shown in Figure 1, an injectable temperature-sensitive hydrogel of 2D MXene nanosheets encapsulated with imiquimod (R837) and cisplatin (DDP) was designed and developed as a local near-infrared (NIR) drug delivery system for local immuno-chemotherapy photothermal treatment of NSCLC (PEG-MXene@DDP@R837@sensitive hydrogel drug-carrier system, MDR@SHDS). Injection of temperature-sensitive hydrogel allows the drug to be applied to specific areas. The hydrogel is warmed up and injected into the tumor tissue as a sol-gel, where it transforms into gel at physiological temperature, and the loaded drug is continuously released from the hydrogel.[22] The intelligent drug release system with NIR light as a switch offers increased possibilities for controlled drug release and sequential therapy. MXene is a new type of 2D nanomaterial with outstanding NIR light absorption and photothermal conversion ability, good biocompatibility, and a large surface area-to-volume ratio. These features make MXene a potential candidate in PTT and drug delivery.[23–25] R837 is a small molecule agonist at Toll-like receptor 7 (TLR-7). It promotes the maturation of DCs and enhances their phagocytosis of tumor cells by activating TLR-7 expressed on DCs.[26,27] However, R837 has a small molecular weight and spreads rapidly to the whole body after injection, resulting in severe immune-related toxicity.[28] DDP kills tumor cells by blocking DNA replication and transcription and is the first-line drug used in NSCLC chemotherapy.[29,30] However, DDP has poor water solubility and low cell permeability.[31] A sensitive hydrogel

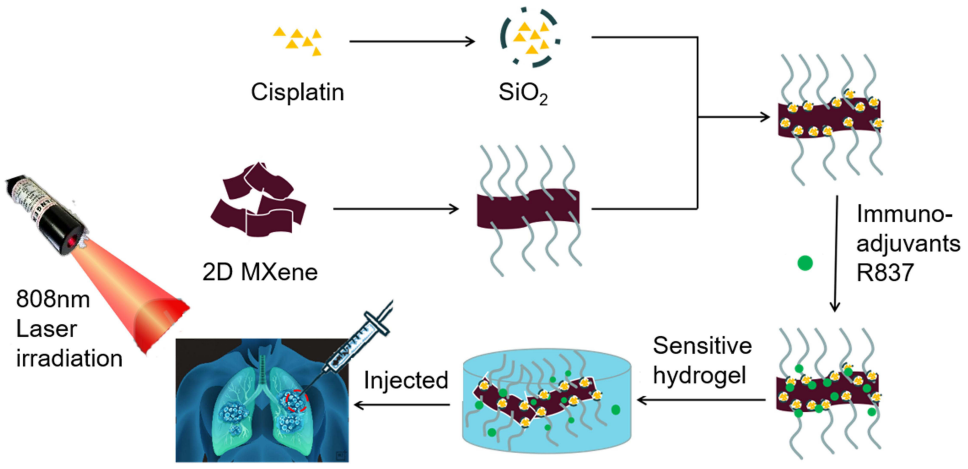

Figure 1 Schematic illustration the of preparation process of MDR@SHDS.

drug-carrier system can control the range of immune activation responses and improve the solubility and utilization of drugs. After the drug was injected into the local tumor tissue, MDR@SHDS transformed from a colloid into a gel. First, the outer layer R837 is released to promote DC maturation and phagocytosis of tumor cells. Then, under the irradiation of NIR light, 2DMXene is used to convert gel into a sol, triggering the internal release of DDP on demand and killing the remaining immune escape tumor cells.

Materials and Methods

Materials

SiO_2, Ti_3C_2-NH_2, DSG-PEG 2000 (98%), low-melting agarose, DDP (Pt 65%), and imiquimod (≥98%, solid) were obtained from Macklin Reagent (Shanghai, China). DMSO and PBS were purchased from Solarbio (Beijing, China). DMEM and fetal bovine serum (FBS) were purchased from BioInd (Israel). Trypsin-EDTA (0.25%), red blood cell lysis buffer, CCK-8 kits, Annexin V-FITC Apoptosis Detection Kits, Edu-488 Cell Proliferation Kits, and TUNEL Apoptosis Assay Kits were purchased from Beyotime Biotechnology (Shanghai, China). All cell lines were obtained from Anhui Laierwen Technology Co. Ltd (Anhui, China).

Synthesis and Characterization of PEG-MXene and PEG-MXene@DDP@R837

Ti_3C_2-NH_2 (50 mg) and DSG-PEG 2000 (100 mg) were dissolved in PBS (10 mL). The solution was magnetically stirred at room temperature for 12 h. The dispersion was then centrifuged for 30 min at 3500 rpm, washed with PBS for three cycles, and vacuum-dried to get rid of PEG-MXene. SiO_2 (50 mg) and DDP (22.5 mg) were dissolved in DMSO (15 mL). The solution was magnetically stirred at room temperature for 12 h. The dispersion was then centrifuged for 30 min at 3500 rpm, washed with DMSO for three cycles, and dissolved in ddH_2O (15 mL). Dried PEG-MXene nanosheets (50 mg) and imiquimod (100 mg) were dissolved in SiO_2 solution (15 mL). The mixture was treated with an ultrasonic bath for 2 h. Thereafter, the dispersion was magnetically stirred at room temperature for 12 h, centrifuged for 30 min at 3500 rpm, washed with ddH_2O for three cycles, and dissolved in ddH_2O (5 mL).

The morphology of PEG-MXene and PEG-MXene@DDP@R837 was characterized using a transmission electron microscope (TEM, FEI Company), and the elements contained were measured using X-ray photoelectron spectroscopy (XPS, Thermo Fisher Scientific).

Synthesis and Characterization of MDR@SHDS

The PEG-MXene@DDP@R837 solution was mixed with 1% agarose solution (15 mL) into MDR@SHDS for further use. The morphology of MDR@SHDS was characterized using TEM, and the elements contained were measured by XPS. The phase transition feature of hydrogel was investigated using the tube inversion method. MDR@SHDS was sealed in a 2 mL test tube and slowly heated from 25°C to 60°C in a water bath. The temperature at which the liquid was mobile within 30s was recorded as the melting temperature.

To test the photothermal stability of the system, ddH_2O, free DDP, free R837, and different concentrations of M@SHDS were added into EP tubes and irradiated with an 808 nm NIR laser at a power density of 2.0 W/cm^2 for 6 min (Beijing Honglan Photoelectric Technology Company). The temperature changes in the sample at different time points were measured using an infrared thermal imaging camera. To test the photothermal stability of M@SHDS and MDR@SHDS, the samples were irradiated with an 808 nm laser for five on/off cycles. The temperature variations before and after irradiation were measured by an infrared thermal imaging camera (HIKMICRO K20 camera, Hangzhou, China).

The controlled release property of the system was also investigated. A 0.1 mL Cy7 solution (0.015 mg/mL) or M@SHDS loaded with equivalent Cy7 was injected into nude mice subcutaneously (Female BALB/c nude mice, 6–8 weeks old). The fluorescence signals were examined at different time points using an optical and X-ray small animal imaging system (In-Vivo Xtreme, Bruker).

In vitro Cytotoxicity

In vitro cytotoxicity was investigated using CCK-8 kits. Mouse lung cell line Lewis and embryonic fibroblast cell line 3T3 were cultured in complete DMEM supplemented with 10% FBS, 1% penicillin, and 1% streptomycin. Macrophage cell line RAW 246.7 was maintained in complete RMPI 1640. Cells were incubated in a humidified incubator at 37°C with 5% CO_2. CCK-8 assays were used to detect the cellular viability of M@SHDS; Lewis, RAW 246.7, and 3T3 cells were seeded in 96-well plates and incubated for 24 h. Then, M@SHDS of various concentrations were added and incubated for another 24 h. CCK-8 solution was used to determine cell cytotoxicity.

Hemolysis Assay

Mouse blood was taken from its eye (Female C57 mice, 6–8 weeks old) and placed into an anticoagulant blood vessel. The blood was centrifuged (3000 rpm, 15 min), and erythrocytes were collected. Then, 0.1 mL of erythrocytes was mixed with MDR@SHDS at various concentrations (25, 50, 75, and 100 μg/mL) and incubated at 37°C for 4 h. The samples were then centrifuged for 15 min at 3000 rpm. The results were recorded by taking photos. The PBS group was a negative control. Erythrocytes mixed with ddH_2O were used for 100% hemolysis. After the samples were centrifuged, the supernatant's absorbance was tested by an automatic microplate reader at 542 nm (Thermo Fisher Scientific). The hemolysis percentage was calculated using the following equation:

$$\text{Hemolysis } (\%) = (I/I_0) \times 100\%$$

where I denote the absorbance value of the experimental group, and I_0 denotes the absorbance value of erythrocytes after complete hemolysis in ddH_2O.

Inflammatory Response

The mice (Female BALB/c mice, 6–8 weeks old) were injected subcutaneously with 0.1 mL M@SHDS and sacrificed at different time points to observe the inflammation around the subcutaneous tissue of the hydrogel area. The subcutaneous tissue was fixed with 4% paraformaldehyde (PFA) and embedded in paraffin overnight. Specimens were cut into 4 mm-thick sections and fixed on the glass slide. Tissue sections were dewaxed, dehydrated, and transparentized, followed by hematoxylin and eosin (H&E) staining and Masson staining. The image of each section was recorded with a microscope (Olympus Company, Japan).

In vitro Cancer Cellular Viabilities, Proliferation, and Apoptosis

To evaluate the ability of M@SHDS to kill cancer cells, with or without PTT, the viability of Lewis cells was measured using CCK-8 assay. Lewis cells were seeded in 96-well plates and incubated for 24 h. Then, MDR@SHDS was added. For NIR treated group, cells were irradiated with 808 nm NIR laser at 2.0 W/cm^2 for 5 min. Each group was then incubated for another 24 h.

Cellular proliferation was investigated by EdU-488. Lewis cells in the logarithmic growth phase were seeded in 24-well plates at a density of 1×105 cells/well, and 500 μL EdU (10μM) culture medium was added to each well after 24 h and incubated at room temperature for 2 h. Next, the cells were fixed in PBS solution containing 4% PFA for 15 min, washed with PBS containing 0.3% Triton X-100 for 15 min, and then rinsed with PBS buffer. The cells were incubated with 1×Click Additive Solution for 30 min in the dark. PBS buffer was rinsed again and 1×DAPI reaction solution was added for 30 min at room temperature in the dark. Finally, positive cells were observed using fluorescence microscopy (Olympus Company, Japan).

Cellular apoptosis was analyzed using the TUNEL assay. Lewis cells in the logarithmic phase were seeded in 24-well plates at a density of 1×105 cells/well. The cells were fixed with 4% PFA after 24 h, stained using a TUNEL apoptosis detection kit according to the instructions, and finally observed using fluorescence microscopy.

Bone Marrow-Derived Dendritic Cell (BMDC) Maturation Assay

BMDCs were first isolated from C57 mice (Female, 6–8 weeks old) and cultured; mice were sacrificed and cells were extracted from the bone marrow of the femur and tibia. The obtained cells were resuspended in red blood cell lysis buffer to deplete erythrocytes and then counted and resuspended in a culture dish with RPMI-1640 complete medium supplemented with 20 ng/mL mouse granulocyte-macrophage colony-stimulating factor (GM-CSF) and 10 ng/mL

mouse IL-4. The culture media were changed every 2 days. After 7 days, the cells which were not adherent and loosely adherent were harvested into DCs.

The upper chamber containing Lewis cells was placed into the transwell system, whose lower chamber was seeded with DCs. Each upper chamber was treated with the following formulations for 48 h: PBS, PTT, M@SHDS, M@SHDS plus PTT, MDR@SHDS, and MDR@SHDS plus PTT. DCs in all groups were collected, washed, and stained with antibodies of PE antimouse CD11b, PB450 antimouse CD80, and FITC antimouse CD86, and then matured DCs were analyzed by flow cytometry (FACSCanto, BD).

In vivo Photothermal Performance

To explore in vivo photothermal performance of M@SHDS, the xenograft tumor model was established by subcutaneously inoculating 0.1 mL of Lewis cells (5*105 cells) into the back of female C57 mice. When the tumor volume reached 100 mm3, following the equation: volume of tumor (mm^3) = 1/2 * length * (width)2, PBS and M@SHDS (15 mg/kg) were intratumorally injected into the mice. After 24 h, the mice were irradiated with an 808 nm laser (2.0 W/cm^2) for 10 min. Temperature changes during irradiation were recorded using infrared thermal imaging (HIKMICRO K20 camera, Hangzhou, China).

In vivo DC Maturation Assay

Female C57 mice bearing Lewis tumors were selected for the DC maturation experiment. When tumors reached 100mm^3 in volume, PBS, MR@SHDS, MD@SHDS, and MDR@SHDS were injected intratumorally. The tumor was irradiated with 808 nm NIR (2.0W/cm^2) for 5 min. Three days after the last injection, mice were sacrificed to harvest lymph nodes to examine DC maturation using flow cytometry.

In vivo Antitumor Efficacy

Female C57 mice bearing Lewis tumors were randomly divided into seven groups: (1) PBS, (2) MR@SHDS, (3) MD@SHDS, (4) MD@SHDS plus PTT, (5) PTT, (6) MDR@SHDS, and (7) MDR@SHDS plus PTT (n=6). The SHDS dose was 15 mg/kg, and the control group was administered PBS in equal volume. For groups 4, 5, and 7, the mice were exposed to an 808 nm laser at the density of 2.0 W/cm^2 for 10 min. For in vivo antitumor study, the tumor volume and body weight variations were measured every other day. The day of treatment was recorded as day 1. Tumor volume was calculated using the following formula:

volume= [length * $(width)^2$]/2

The experimental rats were euthanized on day 13. Following that, the tumors were weighed and used to create H&E and TUNEL staining sections.

In vivo Immune Cell Analysis

Female C57 mice bearing Lewis tumors were selected for the DC maturation experiment. When tumors reached 100mm^3 in volume, PBS, MR@SHDS, MD@SHDS, and MDR@SHDS were injected intratumorally. The tumor was irradiated with 808 nm NIR (2.0 W/cm^2) for 5 min in the NIR treatment group. Six days later, the same formulations were administrated. Mice were sacrificed on day 12; their spleens were harvested and prepared as single-cell suspensions and then stained using antimouse antibodies of anti-CD3-APC, anti-CD8a-PE, and anti-CD4-FITC. The immune effects were analyzed by flow cytometry.

Statistical Analysis

All data in the study were indicated as mean ± standard deviation (SD). The statistical analysis was performed by one-way ANOVA using GraphPad Prism 8 software.

Results

Characterization of PEG-MXene@DDP@R837 and MDR@SHDS

The morphology of PEG-MXene and PEG-MXene@DDP@R837 was characterized by TEM. PEG-MXene had a lateral size of about 50 nm (Figure 2a), and PEG-MXene@DDP@R837 was 80–100 nm in size laterally (Figure 2b). The surface chemical compositions of PEG-MXene and PEG-MXene@DDP@R837 were further characterized by XPS (Figure 2c). The XPS analysis suggests that amino and SiO_2 modified the surface of PEG-MXene. Besides, MDR@SHDS had 89% encapsulation efficiency and 5.9% DDP loading. Figure 2d shows the accumulative diffusion profiles of free DDP and MDR@SHDS. DDP was released more slowly when capsuled with hydrogel. The appearance changes in MDR@SHDS at different temperatures are presented in Figure 2e. The material was solid at 37°C. As the temperature increased, the hydrogel converted into a sol-gel.

Figure 3a-d presents the photothermal performance and stability analysis of M@SHDS and MDR@SHDS. Different groups were irradiated with an 808 nm NIR laser at a density of 2.0 W/cm^2 for 6 min. Compared with ddH_2O, the temperature of M@SHDS and MDR@SHDS increased to almost 50°C within a minute and finally reached about 60°C. With the increase in MDR@SHDS concentration, the temperature increased at an accelerated rate. For 100μg/mL concentrated MDR@SHDS, the temperature reached 50°C within a minute. The heating curves for M@SHDS and MDR@SHDS, analyzing the photothermal stability of the material, are presented in Figure 3e; little temperature changes were observed even after five on/off cycles. These findings show that M@SHDS can be used as a stable nano-hydrogel loading platform to control the release of DDP and R837 by NIR radiation.

The free Cy7 solution and M@SHDS loaded with equivalent Cy7 were subcutaneously injected into nude mice. As shown in Figure 4, the fluorescence intensity of the free Cy7 group and M@SHDS+Cy7 group decreased with time. The fluorescence of the M@SHDS+Cy7 group was significantly more robust than that of the free Cy7 group at and after 24 h, while the fluorescence of the free Cy7 group weakened considerably after 24 h. The results indicate that M@SHDS could effectively prolong the local release of loaded drugs. The sustainable release of M@SHDS helps the loaded drug to maintain a relatively stable drug concentration in vivo for a long time, which can help improve treatment efficiency.

In vitro and in vivo Biocompatibility Assay

Although past studies have concluded that hydrogel has good biocompatibility, it is necessary to evaluate whether the synthetic material is also biosafe. CCK-8 assays were used to test the cellular viability of M@SHDS with Lewis, RAW 246.7, and 3T3. As shown in Figure 5a, Lewis, RAW 246.7, and 3T3 cell lines were cocultured with M@SHDS at

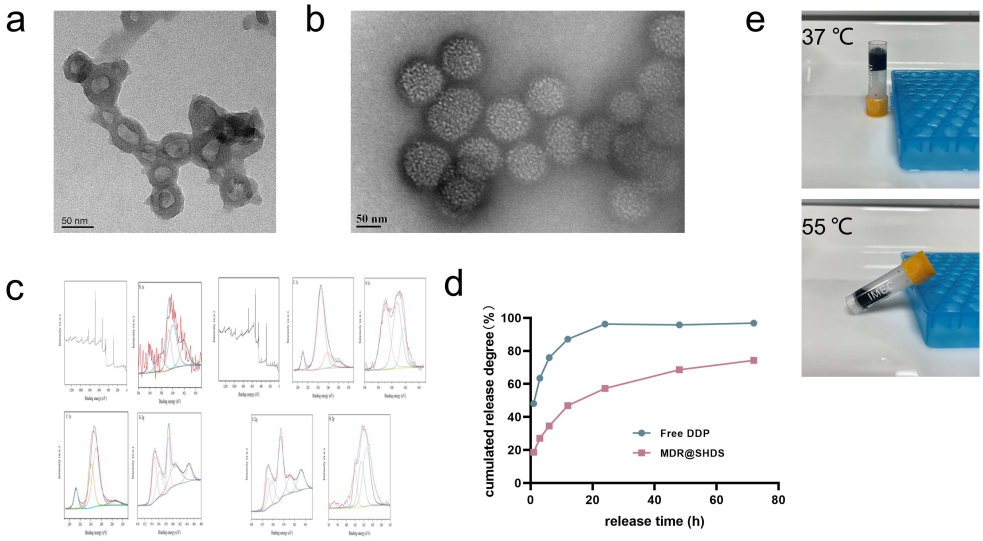

Figure 2 Characterization of PEG-MXene@DDP@R837 and MDR@SHDS. (**a**) TEM of PEG-MXene; (**b**) TEM of PEG-MXene@DDP@R837; (**c**) XPS; (**d**) Controlled release properties of MDR@SHDS; (**e**) The morphology of MDR@SHDS at different temperatures of 37°C and 55°C.

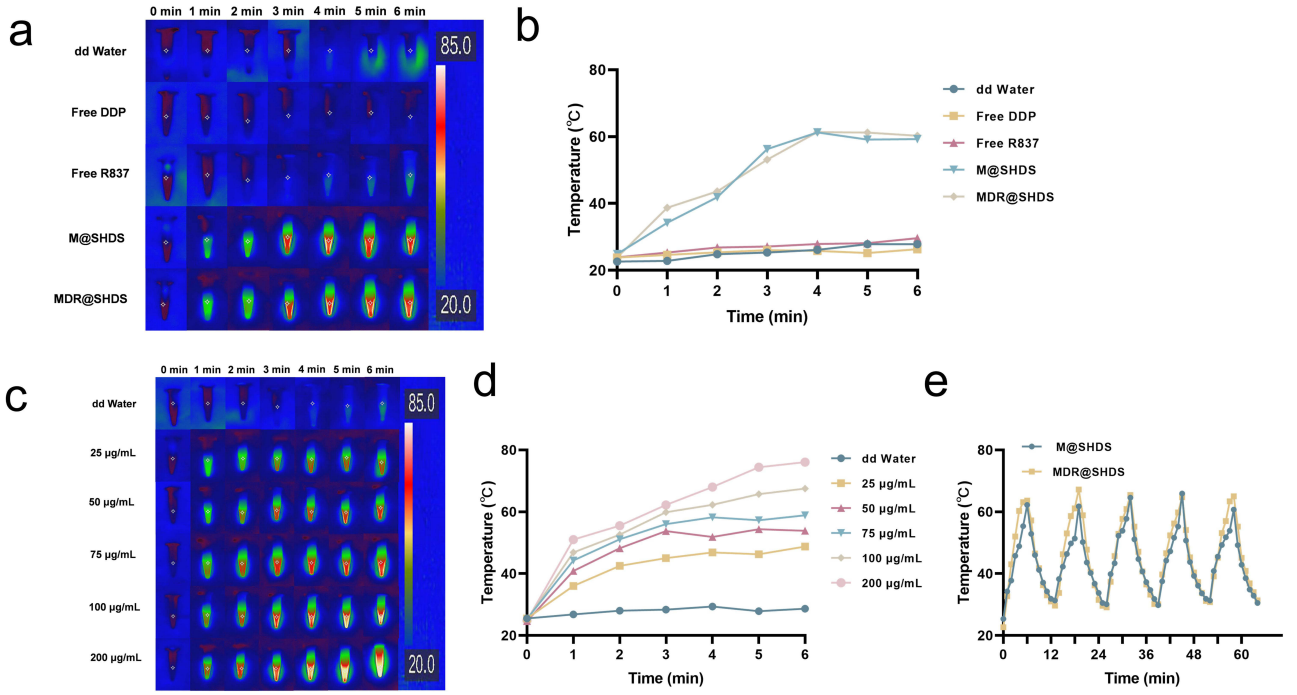

Figure 3 In vitro photothermal performance of MDR@SHDS. (**a** and **b**) The heating curves of different upon 808 nm laser irradiation (2.0 W/cm^2); (**c** and **d**) The heating curves of MDR@SHDS at different concentrations; (**e**) The heating curves upon 5-cycles 808 nm laser exposure (2.0 W/cm ^{2}).

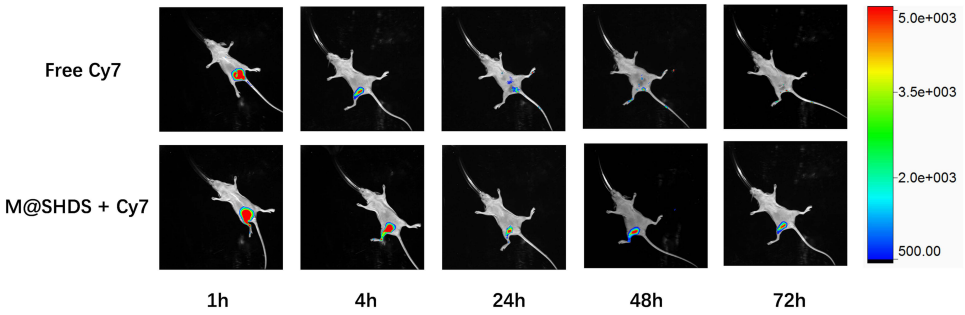

Figure 4 Controlled-release characteristics of M@SHDS. In vivo near-infrared imaging of 0.1 mL, Cy7 solution (0.015 mg/mL), and M@SHDS loaded with equivalent Cy7 in mice subcutaneously at different time points (1 h, 6 h, 24 h, 48 h, 72 h).

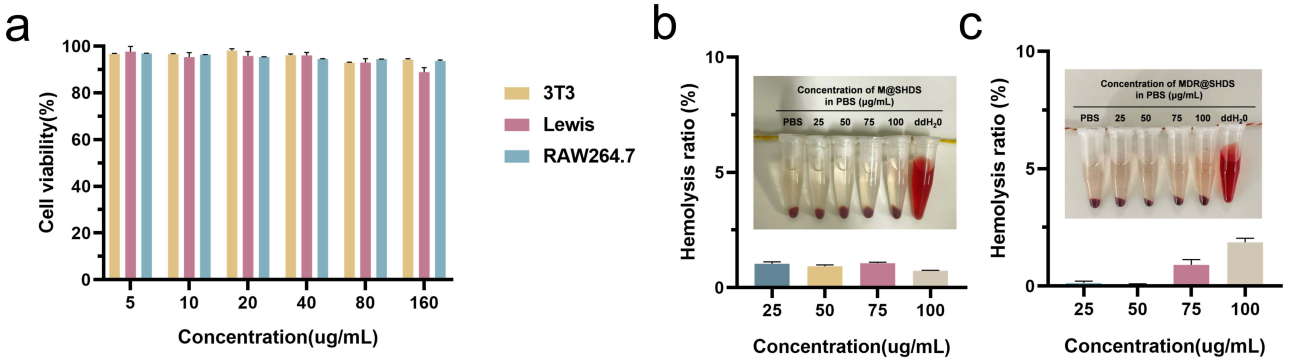

Figure 5 In vitro and in vivo biocompatibility assay. (**a**) Relative cell viabilities of 3T3, Lewis, and RAW264.7 cells exposed to different concentrations of M@SHDS for 24 h; (**b** and **c**) The hemolysis assay of various concentrations of M@SHDS and MDR@SHDS.

https://doi.org/10.2147/IJN.S449541 DovePress

various concentrations for 24 h. After treating the cells with 0–160 μg/mL M@SHDS, the cell viability was higher than 85% and cytotoxicity was very low.

Hemolysis is caused by the rupture of erythrocytes, resulting in the release of hemoglobin into the surrounding fluid.[32] Therefore, hemolysis is often used to evaluate the hemocompatibility of materials.[33] As shown in Figure 5b and c, little hemoglobin leakage was observed from mice RBCs treated with M@SHDS and MDR@SHDS, indicating that few RBCs were destroyed in comparison with the RBCs treated with ddH_2O. The hemolysis rate at various concentrations was less than 2.5%, indicating that the nanomaterial exhibited good biocompatibility with mice RBCs.

Figure 6 shows slight congestion of blood vessels in the subcutaneous tissue of the hydrogel area on the 21st day. The subcutaneous tissue in each group was collected for H&E and Masson staining; we did not observe any infiltrating inflammatory cells or fibrosis in any group, which suggested that M@SHDS did not induce inflammatory cell infiltration and subsequent fibrosis and had good biosafety.

In vitro Cancer Cellular Viabilities, Proliferation, Apoptosis, and DC Maturation Assay

The superior photothermal effect and relatively precise NIR-controlled local drug release of MDR@SHDS motivated us to further explore its potential application in anti-cancer. Cellular viabilities of MDR@SHDS with or without PTT were thus investigated via CCK-8. The results show that the cell viability of MDR@SHDS with the PTT group was significantly inhibited when the nanomaterial concentration exceeded 40 μg/mL (Figure 7a). Edu-488 was used to investigate cell proliferation and further explore the effect of the nanomaterial on tumor cells. The fluorescent dye Edu-488 reacts specifically with proliferating cells, producing green fluorescence. As shown in Figure 7b and c, compared with MDR@SHDS, MDR@SHDS with PTT showed a significant decrease in green fluorescence ($P < 0.01$). The result suggests that PTT leads to more MDR@SHDS-mediated inhibition of cell proliferation.

To evaluate the ability of MDR@SHDS, with or without PTT, to kill lung cancer cells, cell apoptosis in Lewis cells was measured using a TUNEL assay (Figure 8a and b). Compared with the control group, the apoptosis rate was significantly higher in MDR@SHDS with the PTT group ($P < 0.001$).

DCs are the most important APCs that activate T cells and play an essential role in antitumor immunity. CD80 and CD86 are the typical markers to confirm the maturation of DCs.

After 48 hours of treating BMDCs, the percentage of DC maturation was evaluated by flow cytometry (Figure 9a-c). DC maturation rate was the highest in the MDR@SHDS with the PTT group (29.6%). In the absence of NIR, the maturation rate of DC induced by the same dose of MDR@SHDS was slightly lower (25.1%). These results suggest that MDR@SHDS with PTT can induce DC maturation in vitro.

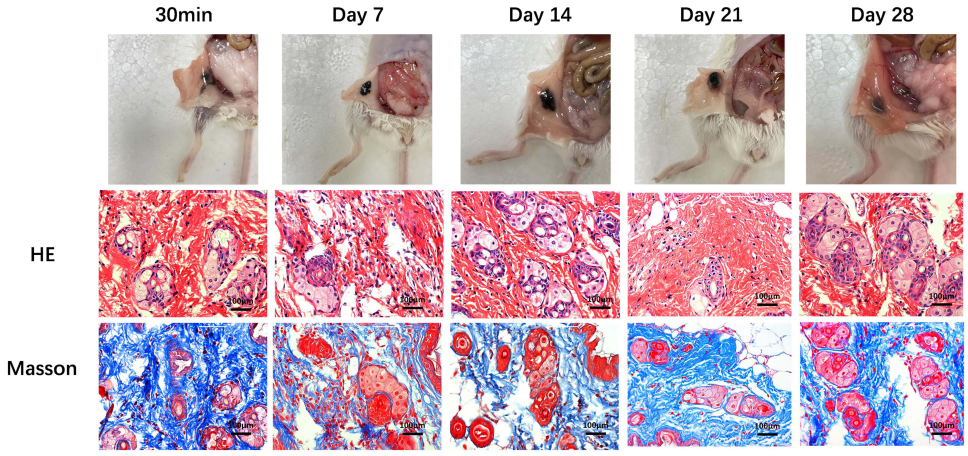

Figure 6 Photographs, HE staining, and Masson staining of M@SHDS in mice subcutaneously at different time points (30 min, Day 7, 14, 21, 28).

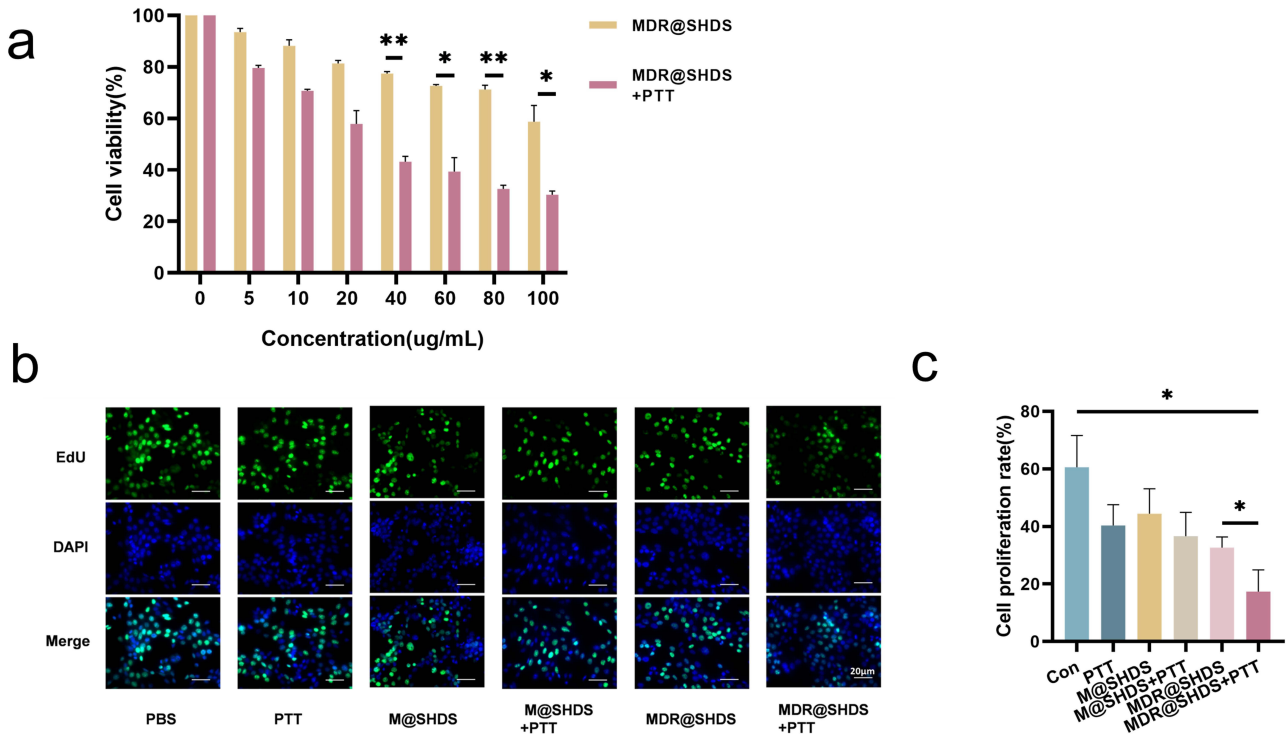

Figure 7 In vitro cancer cellular viabilities, proliferation (**a**) Cellular viabilities of MDR@SHDS with or without PTT (**b** and **c**) EdU fluorescence images after treatment with PTT combined with PBS, M@SHDS, and MDR@SHDS.(The label ** indicates $p < 0.01$, and the label * indicates $p < 0.05$).

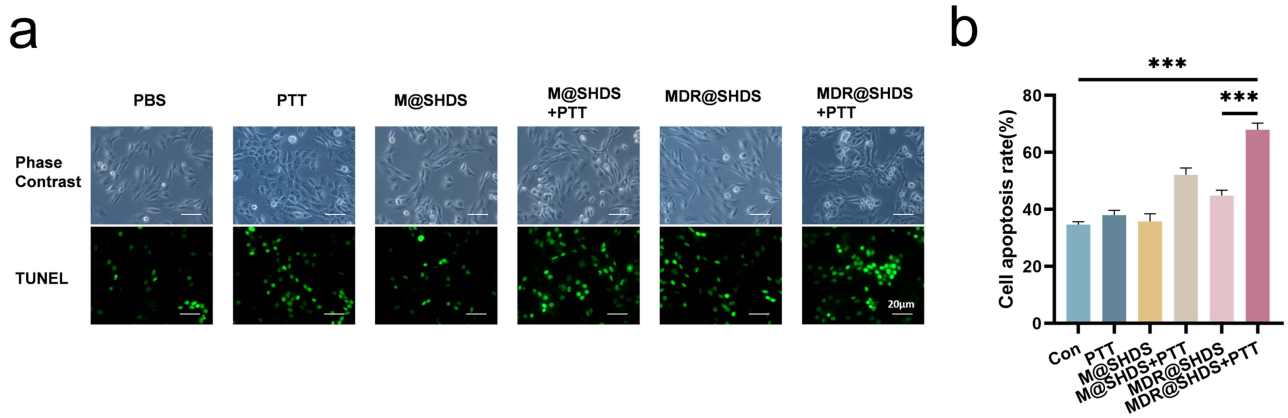

Figure 8 In vitro cancer cellular apoptosis (**a** and **b**) TUNEL fluorescence images after treatment with PTT combined with PBS, M@SHDS, and MDR@SHDS. (The label *** indicates $p < 0.001$).

In vivo Inhibition of Lung Cancer by Photothermal Immuno-Chemotherapy

The in vivo photothermal effect of MDR@SHDS was investigated using C57 tumor-bearing mice. PBS and MDR@SHDS were intratumorally injected into the mice. The mice were irradiated with an 808 nm laser for 10 min at a density of 2.0 W/cm^2. The photothermal images of tumor tissue at different time points are shown in Figure 10. For the MDR@SHDS group, the temperature of tumor tissue increased rapidly and reached about 62°C with NIR exposure, which can effectively kill tumor tissues. The PBS-treated mice exhibited a slow and relatively low-temperature increase after irradiation.

Considering the photothermal effect of MDR@SHDS, we further explored its potential application in antitumor photothermal immuno-chemotherapy.

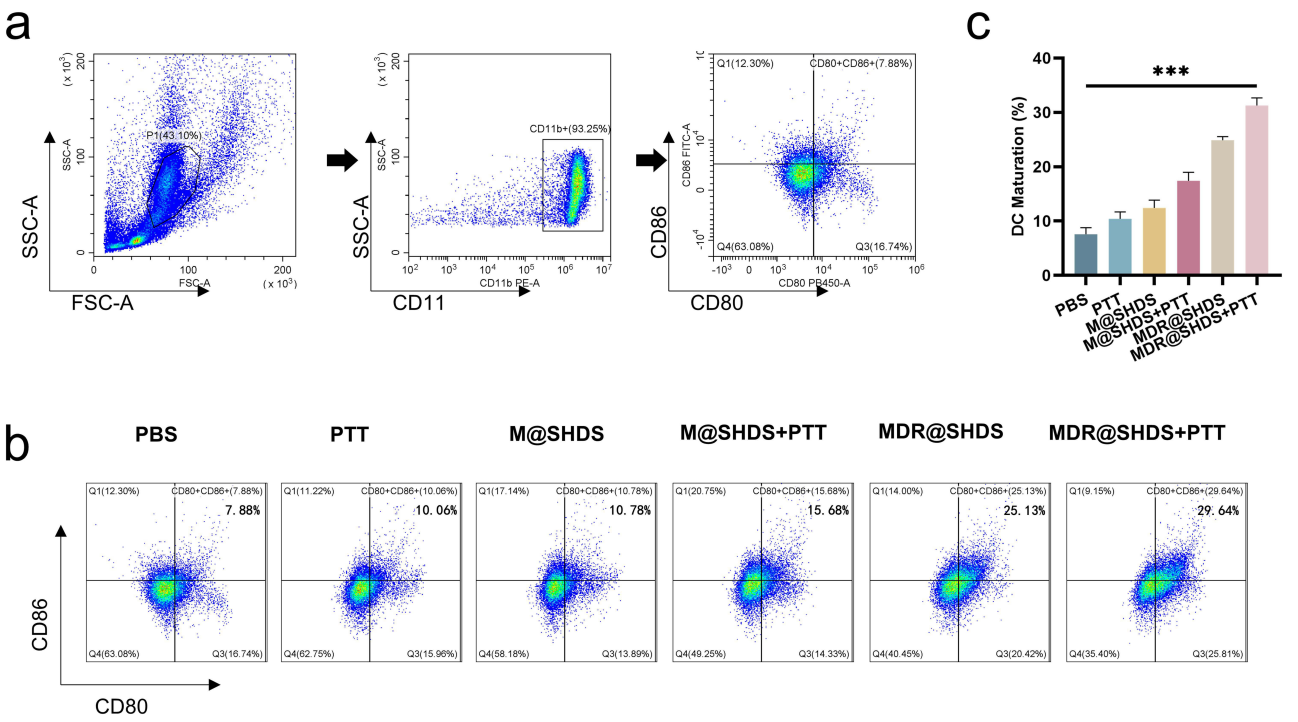

Figure 9 (**a** and **b**) Expression levels of surface molecules (CD80 and CD86) on BMDCs after various treatments; (**c**) Quantification of expression levels of CD80 and CD86 on the surface of BMDCs. (The label *** indicates $p < 0.001$).

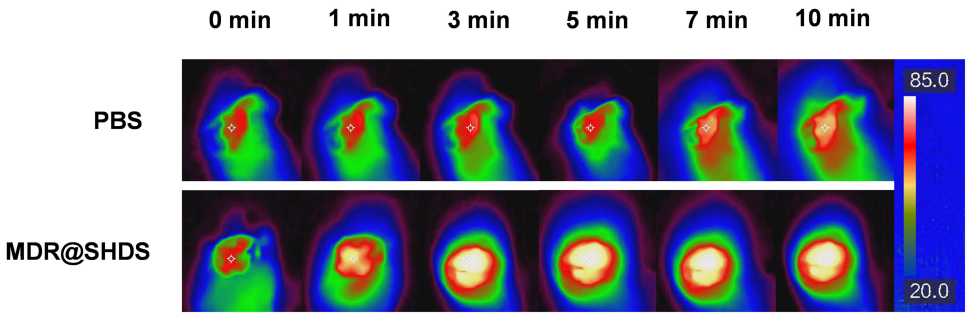

Figure 10 Thermal images of mice bearing tumor after injection of PBS or MDR@SHDS, followed by being exposed to 808 nm irradiation.

As shown in Figure 11a, MDR@SHDS irradiated with an 808 nm laser significantly inhibited tumor growth compared with other control groups. Mice treated with 808 nm laser irradiation alone or MR@SHDS showed a rapid increase in tumor tissue, similar to the PBS group. MD@SHDS without NIR irradiation or MD@SHDS with 808 nm laser irradiation could partially inhibit tumor growth. Furthermore, enhanced therapeutic efficacy was observed for MDR@SHDS with NIR irradiation than without NIR irradiation. This might be because 808 nm laser irradiation not only increased the temperature of the tumor tissue but also triggered the release of DDP inside the nano-hydrogel material. H&E staining of tumor in MDR@SHDS with NIR irradiation indicated significant tissue damage (Figure 11b). These results suggest that MDR@SHDS acts as a mediator in PTT and triggers the release of DDP in tumor tissue, effectively restricting tumor growth.

The change in body weight of mice and H&E staining data of vital tissues were analyzed to evaluate the biocompatibility of this nano-hydrogel system. There was no significant change in the body weight of mice (Figure 12). The heart, liver, spleen, lung, and kidney of mice in each group were stained with H&E; there was no visible tissue damage in any of the organs (Figure 13), indicating high biocompatibility of the system.

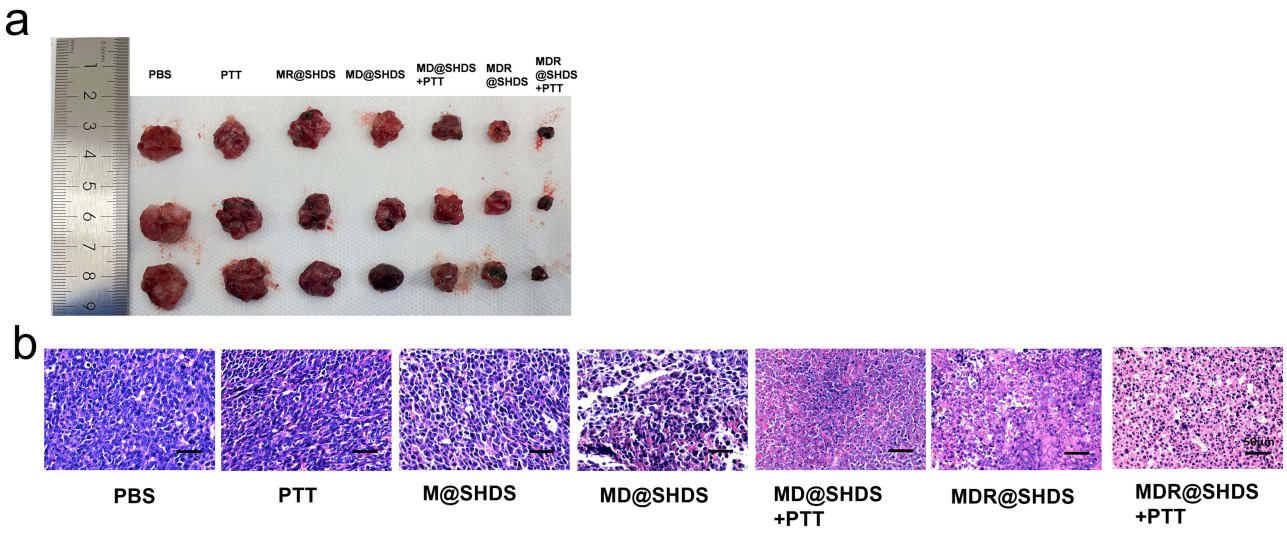

Figure 11 (**a**) Images of tumors at 13 days post-treatment; (**b**) HE stains of tumors at 13 days post-treatment.

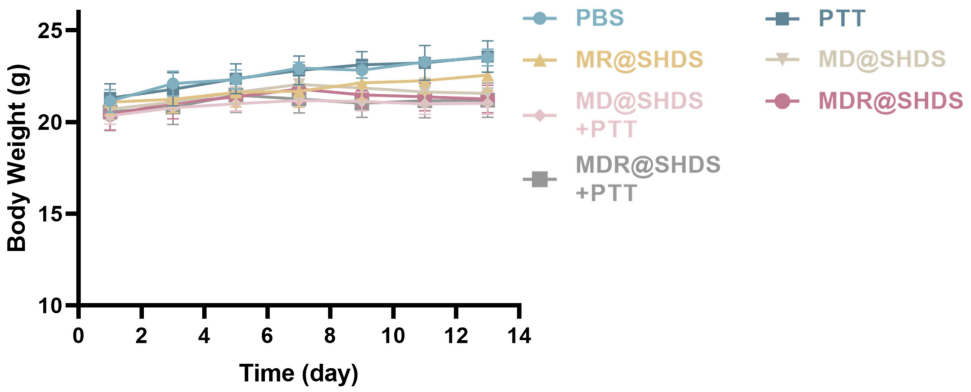

Figure 12 (**a**) Tumor growth curves. (**b**) Body weight changes of C57 mice bearing Lewis tumors were recorded every other day after different treatments.

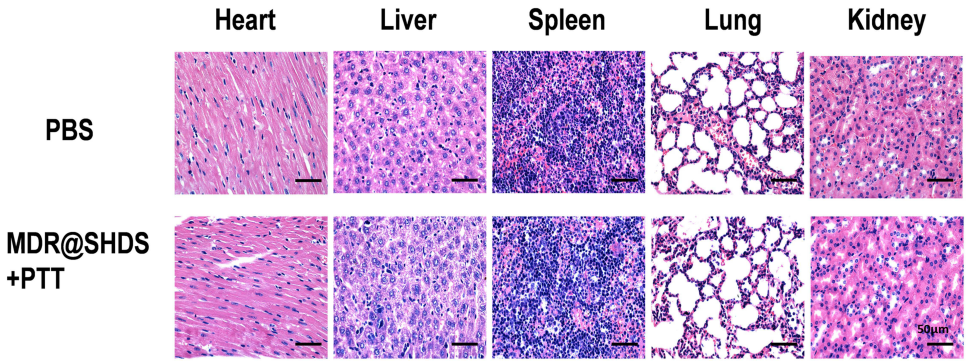

Figure 13 H&E staining of mice heart, liver, spleen, lung, and kidney after PBS and MDR@SHDS treatments.

Flow cytometry test was performed to analyze DC and T cell proliferation and activation to understand the essential immune mechanisms behind the anti-tumor effects of MDR@SHDS with PTT. DC maturation analysis results in vivo are shown in Figure 14a and c. MDR@SHDS with PTT activated 25% of the DCs. In comparison, MDR@SHDS without PTT and other MR@SHDS groups reported a lower DC maturation rate. This shows that MDR@SHDS with PTT can effectively induce DC maturation.

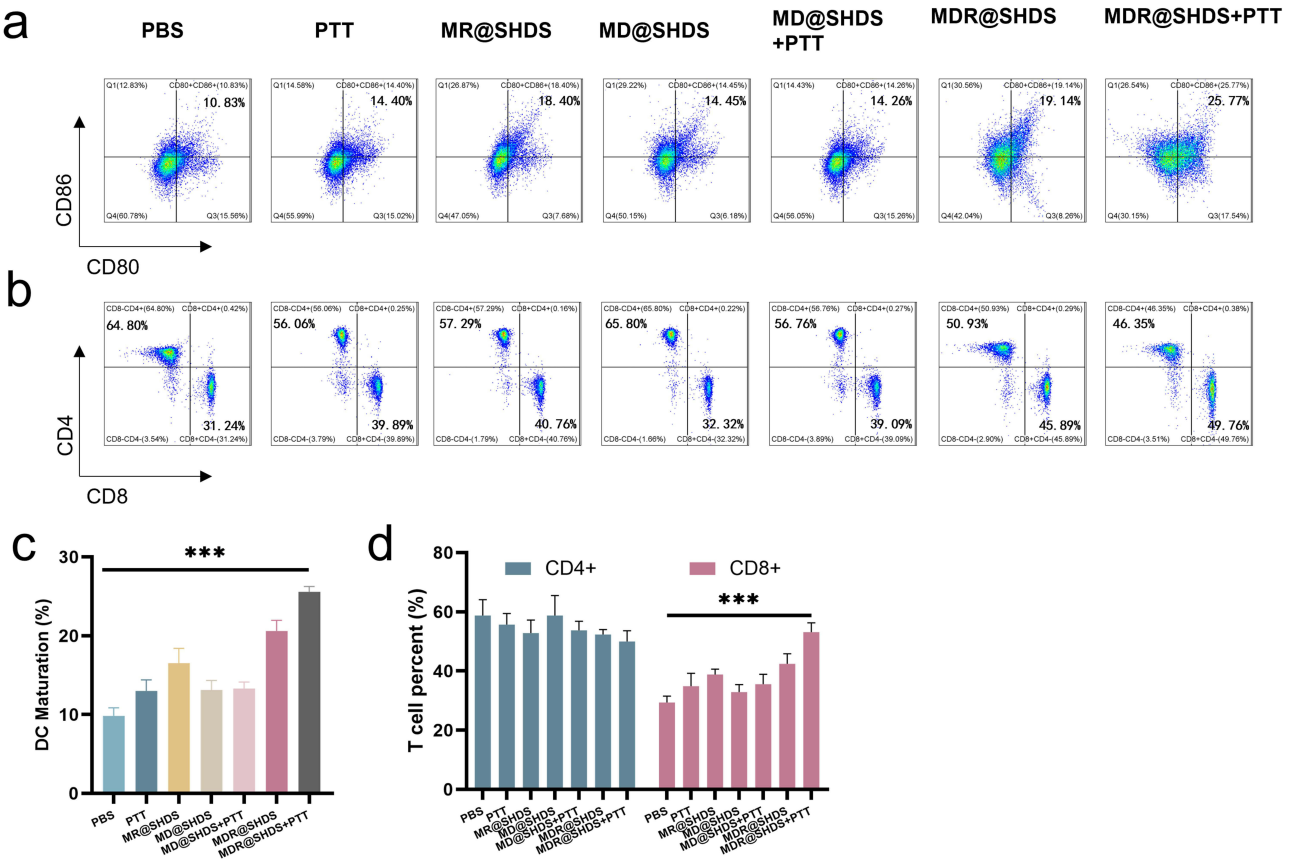

Figure 14 (**a** and **c**) matured DCs in lymph node; (**b** and **d**) cytotoxic $CD8^+$ T cells and $CD4^+$ T cells in spleens after various treatments. (The label *** indicates $p < 0.001$).

Research has proven that $CD8^+$ T lymphocytes are potent tumor immune killer cells and $CD4^+$ T cells usually act in adaptive immune regulation. The spleens of mice in various groups were collected at different temperatures to test the $CD8^+$ and $CD4^+$ T cells by flow cytometry (Figure 14b and d). Compared with the control group, the percentage of $CD8^+$ T cells in MDR@SHDS with PTT dramatically increased. We did not observe a significant increase in $CD4^+$ T cells in the treatment groups (Figure 14b and d).

Discussion

2D Mxene nanosheet is a novel two-dimensional nanomaterial. The first discovery of the MXene material Ti3C2 by Gogotsi et al led to several studies on it due to its graphene-like properties.[34] Its outstanding near-infrared light absorption and photothermal conversion ability, good biocompatibility, and large surface area-to-volume ratio make it promising for biomedical applications such as photothermal therapy, drug delivery, bioimaging, and sensing. Chen et al used hyaluronic acid and Doxorubicin (DOX) to modify Ti3C2 layer by layer to produce Ti3C2-DOX multifunctional nanoplatforms. Ti3C2-DOX was injected into HCT-116 tumor-bearing mice by intravenous drug delivery, and the tumour site was irradiated with an 808-nm near-infrared laser. The temperature of the tumour site in the Ti3C2-DOX injection group increased to 53.1°C within 5 minutes, whereas the temperature of the PBS control group did not change significantly. Observation of the therapeutic effect showed that the Ti3C2-DOX combined with PTT group eliminated the tumour without recurrence.[35] This study provides new ideas for tumour therapy based on 2D Mxene nanosheets and demonstrates the therapeutic potential of 2D Mxene nanosheets.

There have been many studies on the application of 2D MXene nanomaterials for photothermal therapy. However, the use of 2D MXene nanomaterials for encapsulating chemotherapeutic and immunotherapeutic drugs in combination with temperature-sensitive hydrogel technology is relatively new. What we have developed is a NIR-triggered drug release system for local injection of temperature-sensitive hydrogels, which allows targeted delivery of anti-tumour drugs to the

tumour site. Based on the material characterisation results, the temperature-sensitive drug delivery system has good temperature-sensitive and is able to achieve a good controlled release at the site of action. The biocompatibility of MDR@SHDS has been demonstrated by cytotoxicity, haemolysis and inflammation assays. The results of in vitro experiments showed that the MDR@SHDS combined with PTT group could inhibit the proliferation of tumour cells more effectively than the MDR@SHD group alone. In Lewis transplanted tumours, MDR@SHDS also demonstrated a good photothermal effect. In addition, R837 released by MDR@SHDS can induce the maturation of DCs more effectively than that of the control group, thus exerting an effective immuno-anti-tumour effect. Overall, the combination of local immunotherapy, chemotherapy and PTT has better anti-tumour effects than local immunotherapy or chemotherapy alone.

Although the potential of Mxene nanosheets and temperature-sensitive hydrogels has been successfully demonstrated in vitro, further studies are needed to confirm whether they meet the long-term efficacy and safety required for clinical applications. In addition, the synthesis of 2D MXene nanosheets is still in the laboratory stage and further exploration of the formulation and design of 2D Mxene nanosheets and hydrogels is needed to maximize their therapeutic potential if applied on a large scale in the biomedical field.

Conclusions

In this study, we developed a local injectable therapeutic platform by loading multifunctional 2D MXene nanomaterial particles PEG-MXene (composed of immunoadjuvants R837 and DDP) into a thermo-responsive hydrogel. The PEG-MXene@DDP@R837@sensitive hydrogel drug-carrier system showed good photothermal performance, repeated irradiation stability, and excellent biocompatibility. MDR@SHDS with PTT showed potential antitumor efficacy in the lung cancer model. Furthermore, PTT and the loaded immunoadjuvant triggered a strong immune response to inhibit tumor progression. To sum up, this study has demonstrated that the nano-hydrogel is simple to prepare, and its photothermal immuno-chemotherapy property has great potential for the clinical treatment of lung cancer.

Abbreviations

DCs, Dendritic cells; PPT, Photothermal therapy; DDP, Cisplatin; MDR@SHDS, PEG-MXene @DDP@R837@sensitive hydrogel drug-carrier system; M@SHDS, PEG-MXene@ sensitive hydrogel drug-carrier system; MR@SHDS, PEG-MXene@R837@sensitive hydrogel drug-carrier system; MD@SHDS, PEG-MXene @DDP@sensitive hydrogel drug-carrier system; NSCLC, Non-small cell lung cancer; APCs, Antigen-presenting cells; TLR, Toll-like receptor; NIR, Near-infrared; R837, Imiquimod; PBS, Phosphate-Buffered Saline; BMDCs, Bone marrow-derived dendritic cell.

Data Sharing Statement

Any display item and related data are available upon request.

Ethics Approval and Consent

The study was approved and supervised by the animal ethics committee of Bengbu Medical University. All procedures strictly adhere to the guidelines for the care and utilization of experimental animals set forth by Bengbu Medical University.

Acknowledgments

We appreciate the polishing services was provided by Anhui Laierwen Technology Co. Ltd.

Author Contributions

All authors contributed to data analysis, drafting or revising the article, have agreed on the journal to which the article will be submitted, gave final approval of the version to be published, and agree to be accountable for all aspects of the work.

Funding

This work were supported by the 2021 Postgraduate Innovation Program of Bengbu Medical College (No. Byycxz21099), the First Affiliated Hospital of Bengbu Medical College Science Fund for Distinguished Young Scholars (No. 2019BYYFYJQ04), the Natural Science Research Project of Bengbu Medical University (No. 2023byzd059), the Natural Science Research Project of Anhui Educational Committee (Nos. KJ2021A0692 and KJ2021A0781), the Scientific Research Project of Anhui Province of Health Commission (No. AHWJ2021b075).

Disclosure

The authors report no conflicts of interest in this work.

References

1. Siegel RL, Miller KD, Fuchs HE, et al. Cancer statistics, 2022. *CA Cancer J Clin*. 2022;72(1):7–33. doi:10.3322/caac.21708
2. Herbst RS, Morgensztern D, Boshoff C. The biology and management of non-small cell lung cancer. *Nature*. 2018;553(7689):446–454. doi:10.1038/nature25183
3. Vinod SK, Hau E. Radiotherapy treatment for lung cancer: current status and future directions. *Respirology*. 2020;25 Suppl 2:61–71. doi:10.1111/resp.13870
4. Rallis KS, Lai Yau TH, Sideris M. Chemoradiotherapy in Cancer Treatment: rationale and Clinical Applications. *Anticancer Res*. 2021;41(1):1–7. doi:10.21873/anticanres.14746
5. El-Hussein A, Manoto SL, Ombinda-Lemboumba S, et al. A Review of Chemotherapy and Photodynamic Therapy for Lung Cancer Treatment. *Anticancer Agents Med Chem*. 2021;21(2):149–161. doi:10.2174/18715206MTA1uNjQp3
6. Roach MC, Robinson CG, Dewees TA, et al. Stereotactic Body Radiation Therapy for Central Early-Stage NSCLC: results of a Prospective Phase I/II Trial. *J Thorac Oncol*. 2018;13(11):1727–1732. doi:10.1016/j.jtho.2018.07.017
7. Wei Q, Arami H, Santos HA, et al. Intraoperative Assessment and Photothermal Ablation of the Tumor Margins Using Gold Nanoparticles. *Adv Sci*. 2021;8(5):2002788. doi:10.1002/advs.202002788
8. Arroyo-Hernandez M, Maldonado F, Lozano-Ruiz F, et al. Radiation-induced lung injury: current evidence. *BMC Pulm Med*. 2021;21(1):9. doi:10.1186/s12890-020-01376-4
9. Yadav A, Singh S, Sohi H, et al. Advances in Delivery of Chemotherapeutic Agents for Cancer Treatment. *AAPS Pharm Sci Tech*. 2021;23(1):25. doi:10.1208/s12249-021-02174-9
10. Nezhadi S, Saadat E, Handali S, et al. Nanomedicine and chemotherapeutics drug delivery: challenges and opportunities. *J Drug Target*. 2021;29(2):185–198. doi:10.1080/1061186X.2020.1808000
11. Manzari MT, Shamay Y, Kiguchi H, et al. Targeted drug delivery strategies for precision medicines. *Nat Rev Mater*. 2021;6(4):351–370. doi:10.1038/s41578-020-00269-6
12. Xu Y, Hsu JC, Xu L, et al. Nanomedicine-based adjuvant therapy: a promising solution for lung cancer. *J Nanobiotechnology*. 2023;21(1):211. doi:10.1186/s12951-023-01958-4
13. Farhood B, Najafi M, Mortezaee K. CD8(+) cytotoxic T lymphocytes in cancer immunotherapy: a review. *J Cell Physiol*. 2019;234(6):8509–8521. doi:10.1002/jcp.27782
14. Gardner A, De Mingo Pulido A, Ruffell B. Dendritic Cells and Their Role in Immunotherapy. *Front Immunol*. 2020;11:924. doi:10.3389/fimmu.2020.00924
15. Labani-Motlagh A, Ashja-Mahdavi M, Loskog A. The Tumor Microenvironment: a Milieu Hindering and Obstructing Antitumor Immune Responses. *Front Immunol*. 2020;11:940. doi:10.3389/fimmu.2020.00940
16. Ravi Kiran A, Kusuma Kumari G, Krishnamurthy PT, et al. Tumor microenvironment and nanotherapeutics: intruding the tumor fort. *Biomater Sci*. 2021;9(23):7667–7704. doi:10.1039/D1BM01127H
17. Xuan J, Wang Z, Chen Y, et al. Organic-Base-Driven Intercalation and Delamination for the Production of Functionalized Titanium Carbide Nanosheets with Superior Photothermal Therapeutic Performance. *Angew Chem Int Ed Engl*. 2016;55(47):14569–14574. doi:10.1002/anie.201606643
18. Jia Y, Shi K, Yang F, et al. Multifunctional Nanoparticle Loaded Injectable Thermoresponsive Hydrogel as NIR Controlled Release Platform for Local Photothermal Immunotherapy to Prevent Breast Cancer Postoperative Recurrence and Metastases. *Adv Funct Mater* 2020;30.
19. Zhao L, Zhang X, Wang X, et al. Recent advances in selective photothermal therapy of tumor. *J Nanobiotechnology*. 2021;19(1):335. doi:10.1186/s12951-021-01080-3
20. Dou L, Meng X, Yang H, et al. Advances in technology and applications of nanoimmunotherapy for cancer. *Biomark Res*. 2021;9(1):63. doi:10.1186/s40364-021-00321-9
21. Jahanban-Esfahlan R, Derakhshankhah H, Haghshenas B, et al. A bio-inspired magnetic natural hydrogel containing gelatin and alginate as a drug delivery system for cancer chemotherapy. *Int J Biol Macromol*. 2020;156:438–445. doi:10.1016/j.ijbiomac.2020.04.074
22. Dong Y, Li S, Li X, et al. Smart MXene/agarose hydrogel with photothermal property for controlled drug release. *Int J Biol Macromol*. 2021;190:693–699. doi:10.1016/j.ijbiomac.2021.09.037
23. Rohaizad N, Mayorga-Martinez CC, Fojtu M, et al. Two-dimensional materials in biomedical, biosensing and sensing applications. *Chem Soc Rev*. 2021;50(1):619–657. doi:10.1039/d0cs00150c
24. Manisekaran R, Garcia-Contreras R, Rasu Chettiar AD, et al. 2D Nanosheets-A New Class of Therapeutic Formulations against Cancer. *Pharmaceutics*. 2021;13(11). doi:10.3390/pharmaceutics13111803
25. Zhu Y, Tang X, Liu Q, et al. Metallic Carbonitride MXene Based Photonic Hyperthermia for Tumor Therapy. *Small*. 2022;18(22):e2200646. doi:10.1002/smll.202200646

26. Wu Y, Yang Z, Cheng K, et al. Small molecule-based immunomodulators for cancer therapy. *Acta Pharm Sin B*. 2022;12(12):4287–4308. doi:10.1016/j.apsb.2022.11.007
27. Huang L, Ge X, Liu Y, et al. The Role of Toll-like Receptor Agonists and Their Nanomedicines for Tumor Immunotherapy. *Pharmaceutics*. 2022;14(6):1228. doi:10.3390/pharmaceutics14061228
28. Liotti F, Marotta M, Sorriento D, et al. Toll-Like Receptor 7 Mediates Inflammation Resolution and Inhibition of Angiogenesis in Non-Small Cell Lung Cancer. *Cancers*. 2021;13(4):740. doi:10.3390/cancers13040740
29. Bradbury P, Sivajohanathan D, Chan A, et al. Postoperative Adjuvant Systemic Therapy in Completely Resected Non-Small-Cell Lung Cancer: a Systematic Review. *Clin Lung Cancer*. 2017;18(3):259–73 e8. doi:10.1016/j.cllc.2016.07.002
30. Lv P, Man S, Xie L, et al. Pathogenesis and therapeutic strategy in platinum resistance lung cancer. *Biochim Biophys Acta Rev Cancer*. 2021;1876 (1):188577. doi:10.1016/j.bbcan.2021.188577
31. Kadokawa R, Fujie T, Sharma G, et al. High loading of trimethylglycine promotes aqueous solubility of poorly water-soluble cisplatin. *Sci Rep*. 2021;11(1):9770. doi:10.1038/s41598-021-89144-0
32. Shih Y, Venault A, Tayo LL, et al. A Zwitterionic-Shielded Carrier with pH-Modulated Reversible Self-Assembly for Gene Transfection. *Langmuir*. 2017;33(8):1914–1926. doi:10.1021/acs.langmuir.6b03685
33. Hao X, Gai W, Wang L, et al. 5-Boronopicolinic acid-functionalized polymeric nanoparticles for targeting drug delivery and enhanced tumor therapy. *Mater Sci Eng C Mater Biol Appl*. 2021;119:111553. doi:10.1016/j.msec.2020.111553
34. Tang R, Xiong S, Gong D, et al. Ti(3)C(2) 2D MXene: recent Progress and Perspectives in Photocatalysis. *ACS Appl Mater Interfaces*. 2020;12 (51):56663–56680. doi:10.1021/acsami.0c12905
35. Liu G, Zou J, Tang Q, et al. Surface Modified Ti(3)C(2) MXene Nanosheets for Tumor Targeting Photothermal/Photodynamic/Chemo Synergistic Therapy. *ACS Appl Mater Interfaces*. 2017;9(46):40077–40086. doi:10.1021/acsami.7b13421